REGULAR PAPERS

Investigation of electrically active defects in undoped $BaSi_2$ light absorber layers using deep-level transient spectroscopy

Japanese Journal of Applied Physics **57**, 075801 (2018)
https://doi.org/10.7567/JJAP.57.075801

REGULAR PAPER

Investigation of electrically active defects in undoped $BaSi_2$ light absorber layers using deep-level transient spectroscopy

Yudai Yamashita, Takuma Sato, Miftahullatif Emha Bayu, Kaoru Toko, and Takashi Suemasu

Institute of Applied Physics, University of Tsukuba, Tsukuba, Ibaraki 305-8573, Japan

Received January 30, 2018; accepted April 10, 2018; published online June 12, 2018

We grow 500-nm-thick undoped n-$BaSi_2$ epitaxial films on n-Si(111) substrates by molecular beam epitaxy with an optimized Ba-to-Si deposition rate ratio of approximately 2.2, and investigate defect levels and their densities by deep-level transient spectroscopy (DLTS). A hole trap level (H1) with a density $N_T = 1 \times 10^{13}\,cm^{-3}$ is detected at 0.27 eV from the valence band maximum (VBM). It is suggested from a sharp rise in capacitance during trap filling processes that H1 is caused by point defects, which is interpreted to originate from Si vacancies. The leakage current of the diode under reverse-biased voltages increases significantly once the sample temperature exceeds approximately 200 °C during DLTS. Postannealing performed at 200 °C in N_2 for 20 min gives rise to similar results. The measured value of N_T is approximately two orders of magnitude smaller than those reported for undoped $BaSi_2$ films. We also discuss the minimum lifetime of $BaSi_2$ from the viewpoint of the Shockley–Read–Hall recombination model.

1. Introduction

III–V multijunction solar cells composed of stacks of materials with different bandgaps can efficiently utilize the solar spectra and achieve high conversion efficiencies η beyond 40%.[1–5] However, III–V solar cells are relatively expensive and therefore large-scale deployment is not easy. In order to solve this problem, the development of III–V/Si solar cells in which an expensive Ge substrate is replaced with inexpensive Si is in progress.[6] Under these circumstances, we have paid special attention to barium disilicide ($BaSi_2$), which shows great promise as a new material for thin-film solar cells on a Si substrate.[7] $BaSi_2$ is a rare-earth-free and nontoxic semiconductor consisting of Ba and Si, and can be grown epitaxially on a Si(111) substrate with its *a*-axis normal to the substrate surface.[8] It has a suitable bandgap of 1.3 eV, a large optical absorption coefficient of $3 \times 10^4\,cm^{-1}$ for a photon energy of 1.5 eV, which is more than 50 times higher than that of crystalline Si,[9–12] and a large minority carrier diffusion length of about 10 μm.[13] We succeeded in increasing the minority carrier lifetime of undoped $BaSi_2$ epitaxial layers from 0.1 to 10 μs by covering with an amorphous Si (a-Si) layer,[14–16] which is sufficiently large for thin-film solar cells. With the help of a-Si passivation layers, we achieved η approaching 10% in p-$BaSi_2$/n-Si heterojunction solar cells,[17,18] where the p-$BaSi_2$ layer acts as an emitter, and a conduction-band offset $\Delta E_C = 0.85$ eV and a valence-band offset $\Delta E_V = 0.65$ eV at the heterointerface due to the low electron affinity of $BaSi_2$ (3.2 eV),[19] promoting the separation of photogenerated carriers. However, the built-in potential of p-$BaSi_2$/n-Si is as small as 0.1 V. For this reason, the open-circuit voltage (V_{OC}) of p-$BaSi_2$/n-Si solar cells is smaller than 0.5 V.[17,18] Hence, it is not easy to make a drastic improvement in the η of p-$BaSi_2$/n-Si solar cells. To improve η much further, we next target $BaSi_2$ pn homojunction solar cells using an undoped $BaSi_2$ layer as a light absorber layer. Both $V_{OC} > 0.8$ V and $\eta > 25\%$ can be expected for a 2-μm-thick $BaSi_2$ homojunction solar cell.[20] Therefore, the formation of high-quality $BaSi_2$ light absorbers with a low defect density is inevitable.

Deep-level transient spectroscopy (DLTS) is one of the most powerful techniques for detecting electrically active defect levels and their concentrations,[21,22] and has been applied to investigate defect levels in other semiconducting silicides such as β-$FeSi_2$.[23–25] However, there is only one report on the DLTS study of $BaSi_2$.[26] In our previous study,[26] DLTS revealed the presence of majority carrier (electron) traps in undoped n-$BaSi_2$ located at approximately 0.1 and 0.2 eV below the conduction band minimum (CBM). The densities of these trap levels were approximately $1 \times 10^{15}\,cm^{-3}$. Such large defect densities degrade the optical properties of $BaSi_2$. Very recently, we have found that the carrier concentration of undoped $BaSi_2$ changes with a slight deviation of the Ba/Si atomic ratio from stoichiometry.[27] The photoresponsivity drastically changes as a function of the deposition rate ratio of Ba to Si (R_{Ba}/R_{Si}) during molecular beam epitaxy (MBE); it reaches a maximum at $R_{Ba}/R_{Si} = 2.2$. First-principles calculation suggests that Si vacancies are mostly likely to occur as point defects in $BaSi_2$, and that they give rise to localized states within the band gap, leading to the degradation of the minority carrier properties of $BaSi_2$.[27,28] Hence, it is of particular interest to know how the defect levels of $BaSi_2$ and their densities would be improved by optimizing R_{Ba}/R_{Si}.

In this article, we aim to investigate defect levels and their densities in undoped $BaSi_2$ by DLTS. We also discuss the minimum lifetime (τ_{min}) of $BaSi_2$ from the viewpoint of the Shockley–Read–Hall (SRH) recombination model.[29] Photovoltaic absorbers have to be conditioned in such a way that the lifetime of photogenerated carriers is equal to or longer than τ_{min}.

2. Experimental methods

An ion-pumped MBE system equipped with a standard Knudsen cell for Ba and an electron-beam evaporation source for Si was used for the growth. We fabricated a 500-nm-thick undoped n-$BaSi_2$ layer on Czochralski (CZ) n-Si(111) substrates with different resistivities $\rho = 0.1$–1 and 1–4 Ω cm to form a heterojunction diode. The electron concentrations of such n-Si substrates were approximately $n = 5 \times 10^{16}$ and $2 \times 10^{15}\,cm^{-3}$, respectively, while the n of undoped $BaSi_2$ was below $10^{16}\,cm^{-3}$. Although $BaSi_2$ epitaxial layers (*a*-axis-oriented) have three epitaxial variants that rotate by 120° from each other around the surface normal,[30] the grain boundaries (GBs) between the variants do not act as recombination centers.[16,31] As will be described later, the leakage

current in the current density versus voltage (J–V) characteristics under reverse-biased voltages is very large for diodes formed on the n-Si substrate having a low ρ. To systematically investigate the influence of ρ on the J–V characteristics, we formed B-doped p-$BaSi_2$ (300 nm)/n-Si(111) substrates with varying ρ in the range between 0.01–0.1 and 1–4 Ω cm, with the hole concentration of p-$BaSi_2$ fixed at 10^{16} cm^{-3}. Sample preparation was performed as follows: The Si substrate underwent thermal cleaning (TC) at 800 °C under ultrahigh vacuum in addition to the simultaneous deposition of a 1-nm-thick Si layer. With this technique, the defect density in the n-Si substrate became less than 10^{11} cm^{-3}.[32] First, a 50-nm-thick i-Si buffer layer was deposited at 800 °C prior to the formation of $BaSi_2$ layers. Next, we prepared a 5-nm-thick $BaSi_2$ template layer by depositing Ba on an i-Si buffer layer at 500 °C by reactive deposition epitaxy,[33] followed by the codeposition of Ba and Si at 580 °C by MBE to form a 500-nm-thick undoped n-$BaSi_2$ or 300-nm-thick B-doped p-$BaSi_2$ epitaxial layer with an optimized condition of $R_{Ba}/R_{Si} = 2.2$. Finally, a 3-nm-thick a-Si layer was deposited in situ on the surface for surface passivation.[34] The a-Si capping layer suppresses the surface oxidation and behaves as a surface passivation layer. Indium–tin oxide (ITO) electrodes with a diameter of 1 mm and a thickness of 80 nm were sputtered on the surface, and Al electrodes on the entire back surface. For comparison, postannealing was conducted at 200 °C for 20 min in N_2 using a rapid thermal annealing (RTA) system (Thermo Riko MILA-5000-UHV). The postannealing was performed before the electrode deposition. X-ray diffraction (XRD; Rigaku Smart Lab) analysis was used to characterize the crystalline quality of the grown layers. DLTS was carried out in the temperature range of 80–470 K using a 1 MHz capacitance versus voltage (C–V) meter (HP 4280A). The rate window was varied between 1 and 512 ms.

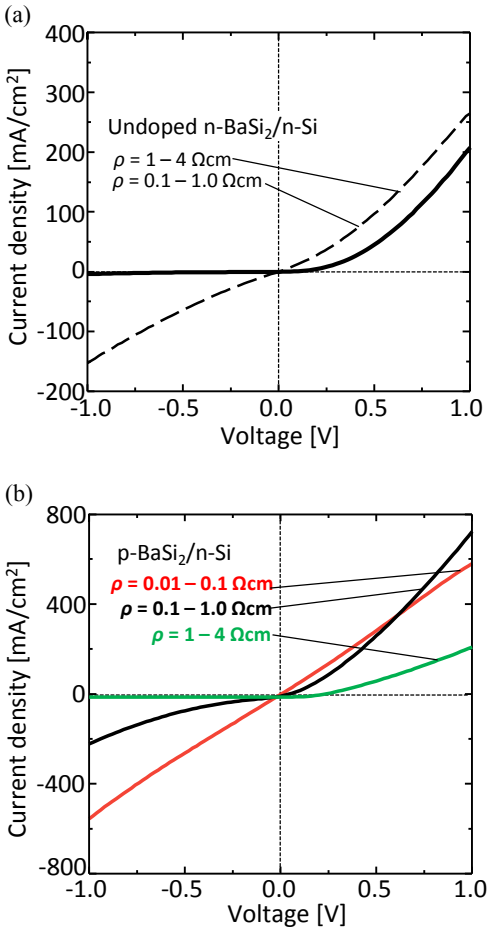

Fig. 1. (Color online) J–V characteristics of (a) undoped n-$BaSi_2$ (500 nm)/n-Si and (b) B-doped p-$BaSi_2$ (300 nm)/n-Si diodes on n-Si substrates having different ρ values.

3. Results and discussion

3.1 Defects in as-grown sample

Voltages were applied to n-Si (p-$BaSi_2$) with respect to n-$BaSi_2$ (n-Si) for the n-$BaSi_2$/n-Si (p-$BaSi_2$/n-Si) diodes. Although both as-grown n-$BaSi_2$/n-Si and p-$BaSi_2$/n-Si diodes exhibited rectifying properties in the J–V characteristics, they degraded as ρ decreased. Figures 1(a) and 1(b) show their representative curves, respectively. For the sample grown on a lower-ρ n-Si substrate, the leakage current under the reverse-bias voltages increased significantly, as shown by the broken line in Fig. 1(a). According to our previous work,[32] step bunching occurs to a far greater extent when a heavily doped (low resistivity $\rho < 0.01$ Ω cm) Si substrate is heated at 900 °C for 30 min in an ultrahigh-vacuum chamber to remove the protective oxide layer on the surface. When ρ is low, step bunching, which causes the generation of defects around the $BaSi_2$/Si heterointerface, cannot be avoided by TC at a reduced temperature of 800 °C. Such large leakage currents make it difficult to evaluate the junction capacitance of the diodes under the reverse-biased condition. On the basis of these results, we chose the sample, i.e., undoped n-$BaSi_2$/n-Si formed on n-Si substrates with ρ = 1–4 Ω cm for DLTS.

A schematic diagram of DLTS is shown in Fig. 2(a). A forward filling pulse voltage (V_P) disturbs the steady-state reverse-bias condition, causing the electric field in the depletion region to decrease. This causes the defect levels to be recharged. When the voltage returns to its steady-state value, the defect levels begin to discharge by emitting trapped carriers by thermal emission, and the resultant time evolution of the capacitance change $\Delta C(T)$ is measured for various rate windows. DLTS allows for the immediate determination of whether the detected defects act as minority or majority carrier traps from the sign of the DLTS signals; positive signals indicate the presence of minority carrier traps, and negative signals indicate the existence of majority carrier traps. The measured DLTS profile of the as-grown sample is shown in Fig. 2(b). The forward filling bias voltage V_P was set at 0.5 V, the pulse width t_{pw} at 100 ms, and the reverse bias voltage V_R at −0.5 V. The electron concentration of $BaSi_2$ is below 10^{16} cm^{-3} and that of the Si substrate is 2×10^{15} cm^{-3} at room temperature. Hence, the depletion region stretches in both sides. However, with a modified pretreatment of the Si substrate, the density of defects in the n-Si region (ρ = 1–4 Ω cm) decreases to a value below the detection limit.[32] For this reason, it is reasonable to suppose that the detected peaks indicate defects in the n-$BaSi_2$ region. In the first experiment denoted by Measurement 1, temperature was increased from 80 to 470 K. An upward facing peak due to minority carrier (hole) traps was observed at approximately 126 K; however, a distinctive change in capacitance ΔC was observed at temperatures higher than 350 K. That is why we performed the second DLTS on the same sample from 80 to

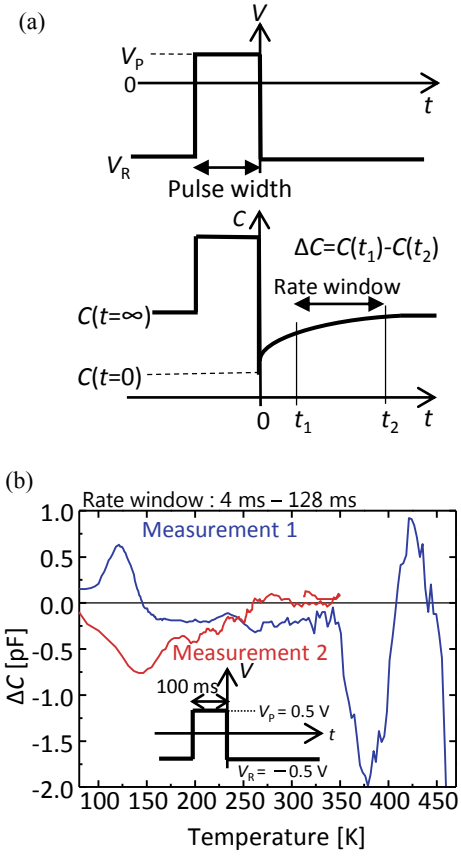

Fig. 2. (Color online) (a) Principle of DLTS and (b) DLTS profiles of as-grown sample obtained under first measurement (Measurement 1) and second measurement (Measurement 2) at $V_P = 0.5$ V, $V_R = -0.5$ V, and $t_{pw} = 100$ ms. The rate window was 4–128 ms.

350 K, which is denoted by Measurement 2. In contrast to that in Measurement 1, a downward facing peak caused by majority carrier (electron) traps was observed at 100–250 K. Once the downward facing peak was observed, the upward facing peak was never detected again. This change is interpreted to originate from the increased temperature up to 470 K (193 °C) during DLTS.

Figure 3 shows the representative J–V characteristics of the diodes measured after the DLTS Measurement 1 (broken line) and after the postannealing without DLTS (dotted line). The degradation of the rectifying properties was also confirmed in the J–V characteristics, showing that the majority carrier traps obtained in DLTS presented in Fig. 2(b) are responsible for the large leakage current at negative bias voltages. To focus on the defect properties of the as-grown sample, we carried out DLTS on another fresh as-grown sample. This time, the measurement temperature was limited up to 300 K to prevent the postannealing effect during the measurement.

Figure 4(a) shows the DLTS profile of the as-grown sample. V_P was set at 0.5 V, and t_{pw} at 50 ms, V_R was varied from −0.5 to −0.1 V. An upward facing peak caused by a minority carrier (holes) trap level (H1) was observed at approximately 126 K in Fig. 4(a). The hole trap level was calculated to be approximately 0.27 eV from the valence band maximum (VBM) in Fig. 4(b), and the defect density N_T was 1×10^{13} cm^{-3}. This value is approximately two orders of magnitude smaller than that previously reported in undoped

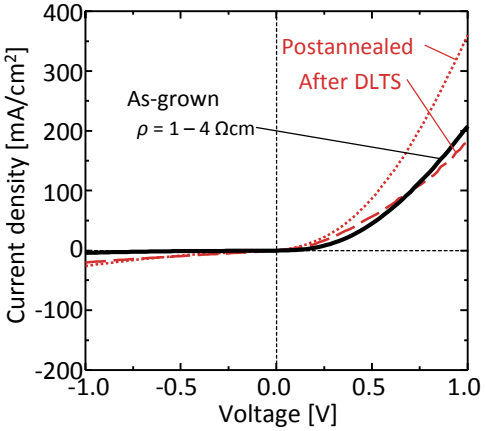

Fig. 3. (Color online) J–V characteristics of undoped n-$BaSi_2$ (500 nm)/n-Si diodes on an n-Si substrate ($\rho = 1$–$4\,\Omega$cm) measured after DLTS (Measurement 1) with temperatures swept from 80 to 470 K (broken line), and after the postannealing at 200 °C in N_2 for 20 min (dotted line).

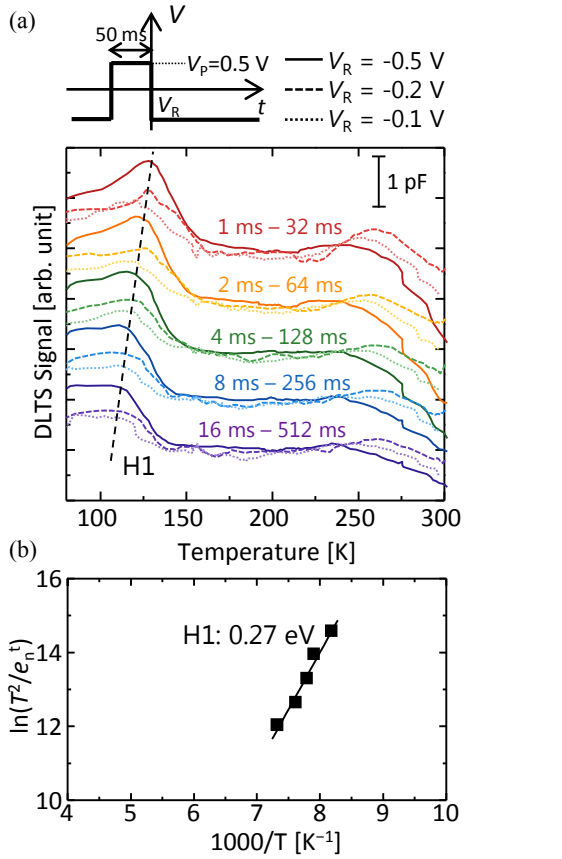

Fig. 4. (Color online) (a) DLTS profiles of as-grown sample at $V_P = 0.5$ V and $t_{pw} = 50$ ms. V_R was varied as −0.5, −0.2, and −0.1 V. The rate window was varied as 1–32, 2–64, 4–128, 8–256, and 16–512 ms. (b) Arrhenius plot for hole trap level (H1).

n-$BaSi_2$ grown with $R_{Ba}/R_{Si} \sim 3$.[26] The DLTS signal intensity observed at approximately 100–125 K decreased as $|V_R|$ decreased from 0.5 to 0.1 V, indicating that the defect density decreased when it approached the interface and therefore the presence of defects in the bulk region of $BaSi_2$. To investigate whether the hole trap level H1 was caused by point or extensive defects, we changed t_{pw} from 0.01 to 800 ms, and measured the signals at 126 K, as shown in Fig. 5(a). The

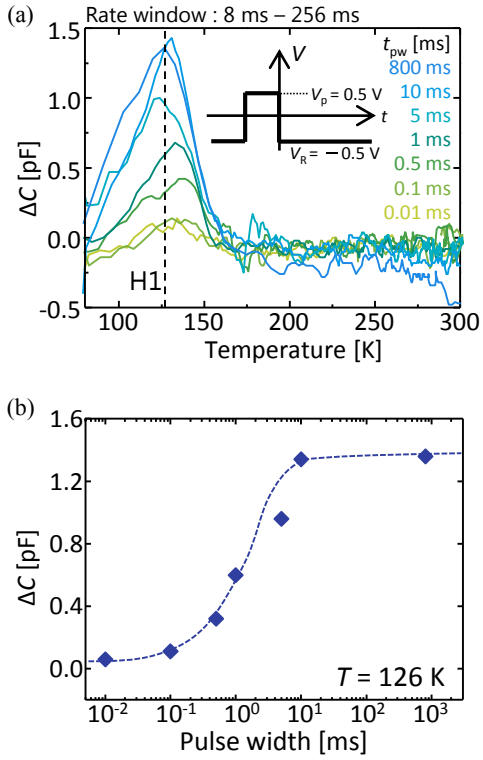

Fig. 5. (Color online) (a) DLTS profiles obtained at different t_{pw} values from 0.01 to 800 ms and (b) dependence of the DLTS signal ΔC on pulse width of V_P, measured at 126 K.

DLTS signal $\Delta C(T)$ increased sharply as t_{pw} increased from 0.1 to 10 ms in Fig. 5(b), which is caused by the presence of point defects.[35] $BaSi_2$ has six types of native point defects: silicon vacancies (V_{Si}), barium vacancies (V_{Ba}), silicon substituted for barium antisites (Si_{Ba}), barium substituted for silicon antisites (Ba_{Si}), silicon interstitials (Si_i), and barium interstitials (Ba_i). First-principles calculation revealed that V_{Si} is most likely to occur from the viewpoint of formation energy in these native point defects.[28] One of the calculated defect levels due to V_{Si} is in good agreement with H1. Takabe et al.[32] found from Rutherford backscattering spectrometry that the Si atomic ratio in the $BaSi_2$ films increased around the $BaSi_2$/Si interface. We therefore suppose that the decrease in defect density around the $BaSi_2$/Si interface presented in Fig. 4(a) is ascribed to the reduction in the density of V_{Si} by the diffusion of Si atoms from the Si substrate into $BaSi_2$. However, we cannot distinguish V_{Si} from other defects by DLTS alone. Thus, more studies are needed to verify this assumption.

3.2 Discussion on minimum SRH lifetime

We next discuss how the defect density on the order of $10^{13}\,cm^{-3}$ detected in this work would affect the optical properties of $BaSi_2$ from the viewpoint of SRH recombination. The τ_{min} condition follows from the requirement of light absorption in relation to charge transport; it is obtained when the capture rates are maximum. In this situation, the τ_{min} of electrons and holes can be described by Eq. (1) under the assumption of equal capture cross sections σ for electrons and holes:[36]

$$\tau_{min} = \frac{1}{\sigma v_{th} N_T}. \quad (1)$$

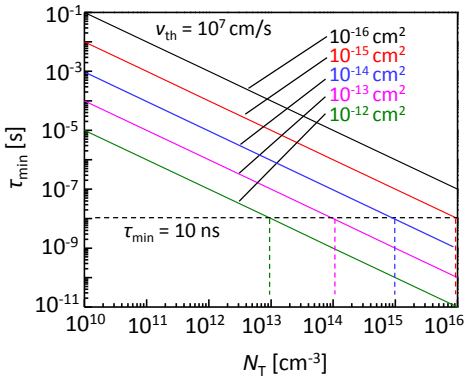

Fig. 6. (Color online) Dependence of minimum SRH lifetime on N_T under the assumption of equal capture cross sections for electrons and holes being in the range between 10^{-12} and $10^{-16}\,cm^2$. τ_{min} is supposed to be 10 ns for $BaSi_2$.

Here, the carrier thermal velocity v_{th} is approximated to be 10^7 cm/s. The capture cross sections of traps can be understood as the extension of a trap perpendicular to the direction of motion of a free charge carrier. Since it is not easy to evaluate σ from the present DLTS profiles, we assumed σ to be in the range between 10^{-12} and $10^{-16}\,cm^2$. Figure 6 shows the τ_{min} versus N_T plot. We estimate the τ_{min} for $BaSi_2$ as follows. In the light-absorbing layer of the solar cell, three times the reciprocal of the light absorption coefficient is necessary to absorb the light sufficiently. Similarly, the minority carrier diffusion length L needs to be longer than this. Therefore, τ_{min} is obtained as[36]

$$\tau_{min} = \frac{9}{D\alpha^2}. \quad (2)$$

Here, D is the diffusion coefficient of carriers and is practically constant for carrier densities below about $10^{17}\,cm^{-3}$.[36] Assuming that $3/\alpha$ is 1 μm and D is $1\,cm^2/s$ for $BaSi_2$,[20] τ_{min} is calculated to be 10 ns. In Fig. 6, τ_{min} (10 ns) is reached at $N_T = 10^{13}\,cm^{-3}$ for undoped $BaSi_2$ at $\sigma = 10^{-12}\,cm^2$. However, the capture cross sections of gap states are usually much smaller than this value ($10^{-12}\,cm^2$), which is reported to be 10^{-18}–$10^{-16}\,cm^2$ in a-Si:H[37] and 10^{-16}–$10^{-15}\,cm^2$ in GaAs (EL2).[38,39] Hence, the condition of $\sigma = 10^{-12}\,cm^{-2}$ is very harsh for $BaSi_2$ and is not likely to occur. On the basis of these discussions, we conclude that the defect density of about $10^{13}\,cm^{-3}$ present in $BaSi_2$ does not significantly affect the minority carrier properties of $BaSi_2$.

4. Conclusions

We grew 500-nm-thick undoped n-$BaSi_2$ epitaxial layers by MBE with an optimized condition of $R_{Ba}/R_{Si} = 2.2$ and investigated defect levels by DLTS. The as-grown sample had a hole trap level (H1) of 0.27 eV from the VBM, and the density was approximately $10^{13}\,cm^{-3}$. This value was approximately two orders of magnitude smaller than that previously reported. This trap level was supposed to be caused by Si vacancies in $BaSi_2$ because its density decreased close to the $BaSi_2$/Si interface. From the viewpoint of SRH recombination, a defect density on the order of $10^{13}\,cm^{-3}$ does not have a detrimental influence on the minority carrier properties of $BaSi_2$.

Acknowledgements

This work was financially supported by JSPS KAKENHI Grant Numbers 15H02237 and 17K18865, and JST MIRAI.

1) M. A. Green, Y. Hishikawa, W. Warta, E. D. Dunlop, D. H. Levi, J. Hohl-Ebinger, and A. W. H. Ho-Baillie, Prog. Photovoltaics **25**, 668 (2017).
2) F. Dimroth, M. Grave, P. Beutel, U. Fiedeler, C. Karcher, T. N. D. Tibbits, E. Oliva, G. Siefer, M. Schachtner, A. Wekkeli, A. W. Bett, R. Krause, M. Piccin, N. Blanc, C. Drazek, E. Guiot, B. Ghyselen, T. Salvetat, A. Tauzin, T. Signamarcheix, A. Dobrich, T. Hannappel, and K. Schwarzburg, Prog. Photovoltaics **22**, 277 (2014).
3) W. Guter, J. Schöne, S. P. Philipps, M. Steiner, G. Siefer, A. Wekkeli, E. Welser, E. Oliva, A. W. Bett, and F. Dimroth, Appl. Phys. Lett. **94**, 223504 (2009).
4) T. Takamoto, E. Ikeda, H. Kurita, M. Ohmori, M. Yamaguchi, and M.-J. Yang, Jpn. J. Appl. Phys. **36**, 6215 (1997).
5) R. R. King, D. Bhusari, D. Larrabee, X.-Q. Liu, E. Rehder, K. Edmondson, H. Cotal, R. K. Jones, J. H. Ermer, C. M. Fetzer, D. C. Law, and N. H. Karam, Prog. Photovoltaics **20**, 801 (2012).
6) T. J. Grassman, D. J. Chmielewski, S. D. Carnevale, J. A. Carlin, and S. A. Ringel, IEEE J. Photovoltaics **6**, 326 (2016).
7) T. Suemasu and N. Usami, J. Phys. D **50**, 023001 (2017).
8) R. A. McKee, F. J. Walker, J. R. Conner, and R. Raj, Appl. Phys. Lett. **63**, 2818 (1993).
9) K. Toh, T. Saito, and T. Suemasu, Jpn. J. Appl. Phys. **50**, 068001 (2011).
10) D. B. Migas, V. L. Shaposhnikov, and V. E. Borisenko, Phys. Status Solidi B **244**, 2611 (2007).
11) M. Kumar, N. Umezawa, and M. Imai, J. Appl. Phys. **115**, 203718 (2014).
12) M. Kumar, N. Umezawa, and M. Imai, Appl. Phys. Express **7**, 071203 (2014).
13) M. Baba, K. Toh, K. Toko, N. Saito, N. Yoshizawa, K. Jiptner, T. Sakiguchi, K. O. Hara, N. Usami, and T. Suemasu, J. Cryst. Growth **348**, 75 (2012).
14) K. O. Hara, N. Usami, K. Toh, M. Baba, K. Toko, and T. Suemasu, J. Appl. Phys. **112**, 083108 (2012).
15) K. O. Hara, N. Usami, K. Nakamura, R. Takabe, M. Baba, K. Toko, and T. Suemasu, Appl. Phys. Express **6**, 112302 (2013).
16) R. Takabe, K. O. Hara, M. Baba, W. Du, N. Shimada, K. Toko, N. Usami, and T. Suemasu, J. Appl. Phys. **115**, 193510 (2014).
17) D. Tsukahara, S. Yachi, H. Takeuchi, R. Takabe, W. Du, M. Baba, Y. Li, K. Toko, N. Usami, and T. Suemasu, Appl. Phys. Lett. **108**, 152101 (2016).
18) S. Yachi, R. Takabe, K. Toko, and T. Suemasu, Appl. Phys. Lett. **109**, 072103 (2016).
19) T. Suemasu, K. Morita, M. Kobayashi, M. Saida, and M. Sasaki, Jpn. J. Appl. Phys. **45**, L519 (2006).
20) T. Suemasu, Jpn. J. Appl. Phys. **54**, 07JA01 (2015).
21) D. V. Lang, J. Appl. Phys. **45**, 3023 (1974).
22) F. Hasegawa, N. Iwata, and Y. Nannichi, Jpn. J. Appl. Phys. **21**, 1479 (1982).
23) M. A. Lourenço, T. M. Butler, A. K. Kewell, R. M. Gwilliam, K. J. Kirkby, and K. P. Homewood, Nucl. Instrum. Methods Phys. Res., Sect. B **175–177**, 159 (2001).
24) A. Tsormpatzoglou, D. H. Tassis, C. A. Dimitriadis, L. Dozsa, N. G. Galkin, D. L. Goroshko, V. O. Polyarnyi, and E. A. Chusovitin, J. Appl. Phys. **100**, 074313 (2006).
25) H. Kawakami, M. Suzuno, K. Akutsu, J. Chen, K. Jiptner, T. Sekiguchi, and T. Suemasu, Jpn. J. Appl. Phys. **50**, 041303 (2011).
26) H. Takeuchi, W. Du, M. Baba, R. Takabe, K. Toko, and T. Suemasu, Jpn. J. Appl. Phys. **54**, 07JE01 (2015).
27) R. Takabe, T. Deng, K. Kodama, Y. Yamashita, T. Sato, K. Toko, and T. Suemasu, J. Appl. Phys. **123**, 045703 (2018).
28) M. Kumar, N. Umezawa, W. Zhou, and M. Imai, J. Mater. Chem. A **5**, 25293 (2017).
29) W. Shockley and W. T. Read, Jr., Phys. Rev. **87**, 835 (1952).
30) Y. Inomata, Y. Nakamura, T. Suemasu, and F. Hasegawa, Jpn. J. Appl. Phys. **43**, L478 (2004).
31) M. Baba, M. Kohyama, and T. Suemasu, J. Appl. Phys. **120**, 085311 (2016).
32) Y. Yamashita, S. Yachi, R. Takabe, T. Sato, M. E. Bayu, K. Toko, and T. Suemasu, Jpn. J. Appl. Phys. **57**, 025501 (2018).
33) Y. Inomata, T. Nakamura, T. Suemasu, and F. Hasegawa, Jpn. J. Appl. Phys. **43**, 4155 (2004).
34) R. Takabe, S. Yachi, W. Du, D. Tsukahara, H. Takeuchi, K. Toko, and T. Suemasu, AIP Adv. **6**, 085107 (2016).
35) E. Simoen, D. Visalli, M. Van Hove, M. Leys, P. Favia, H. Bender, G. Borghs, A. P. D. Nguyen, and A. Stesmans, Phys. Status Solidi A **209**, 1851 (2012).
36) F. T. Dittrich, *Materials Concepts for Solar Cells* (Imperial College Press, London, 2015) Chap. 3.
37) H. Okushi, Y. Tokumaru, S. Yamasaki, H. Oheda, and K. Tanaka, Phys. Rev. B **25**, 4313 (1982).
38) D. C. Look and Z. Q. Fang, J. Appl. Phys. **80**, 3590 (1996).
39) M. A. Zaidi, H. Maaref, and J. C. Bourgoin, Appl. Phys. Lett. **61**, 2452 (1992).